Design Method of Tunable Pixel with Phase-Change Material for Diffractive Optical Elements

Seung-Yeol Lee, Han Na Kim, Yong Hae Kim, Tae-Youb Kim, Seong-Mok Cho, Han Byeol Kang, and Chi-Sun Hwang

In this paper, we propose a scheme for designing a tunable pixel layer based on a $Ge_2Sb_2Te_5$ (GST) alloy thin film. We show that the phase change of GST can significantly affect the reflection characteristic when the GST film is embedded into a dielectric encapsulation layer. We investigate the appropriate positions of the GST film within the dielectric layer for high diffraction efficiency, and we prove that they are antinodes of Fabry–Perot resonance inside the dielectric layer. Using the proposed scheme, we can increase the diffraction efficiency by about ten times compared to a bare GST film pixel, and 80 times for the first-to-zeroth-order diffraction power ratio. We show that the proposed scheme can be designed alternatively for a broadband or wavelength-selective type by tuning the dielectric thickness, and we discuss a multi-phase example with a double-stack structure.

Keywords: Diffraction gratings, $Ge_2Sb_2Te_5$, Phase-Change material, Fabry–Perot resonance, Spatial light modulator.

I. Introduction

Thermally driven phase-change materials, such as vanadium dioxide (VO_2) and germanium antimony tellurium alloy ($Ge_2Sb_2Te_5$, GST), have been extensively researched for their potential application to the design of integrated active optical elements [1] or tunable metamaterials [2]. They have been considered owing to the large variation in the refractive indexes between their phase states. For example, VO_2 can change its optical characteristics from a semiconductor to a metallic phase at near 68 °C [3], and it can therefore easily change its reflectance at a relatively low temperature. Templates for various active plasmonic structures such as tunable nanoantennas [3], [4], perfect light absorbers [5], and split-ring resonators [6], which are developed by depositing or patterning VO_2 structures on a noble metal film, have been reported.

In contrast, a GST alloy exhibits phase-change characteristics from an amorphous to a crystalline state when heated to the range 100 °C to 150 °C [7], [8]. Compared to VO_2, the phase change is maintained even when the alloy cools to room temperature, and is far more stable and effective for power-consumption issues. The phase-change mechanism is repetitive, and is also applicable to both electrical and optical heating [9], [10]. These benefits make GST a key material in various industrial and scientific applications, not only for conventional optical data storage media such as DVDs, but also for highly integrated all-optical multi-level memory [11] and broadband perfect absorbers operated for near-infrared light [12].

In particular, spatial light modulation through GST-based structures has been recently reported for super-resolution optical micro-images [13]. Compared to conventional spatial light modulator (SLM) techniques based on a liquid crystal layer [14] or the mechanical modulation of digital mirrors [15],

Manuscript received Mar. 6, 2016; revised Dec. 6, 2016; accepted Dec. 14, 2016. This work was supported by "The Cross-Ministry Giga KOREA Project" grant from the Ministry of Science, ICT and Future Planning, Korea.

Seung-Yeol Lee (corresponding author, seungyeol@knu.ac.kr) is with the School of Electronics Engineering, Kyungpook National University, Daegu, Rep. of Korea.

Han Na Kim (khn0101@etri.re.kr), Yong Hae Kim (yhakim@etri.re.kr), Tae-Youb Kim (youby@etri.re.kr), Seong-Mok Cho (smcho@etri.re.kr), Han Byeol Kang (khb30348@etri.re.kr.), and Chi-Sun Hwang (hwang-cs@etri.re.kr) are with the ICT Material & Components Research Laboratory, ETRI, Daejeon, Rep. of Korea.

the spatial change of a GST-based structure can be highly integrated below the sub-micron scale through a local phase transformation [16], [17]. The phase change of an extremely thin GST film results in a dramatic change in reflected color [13]. Moreover, a perfect tunable absorber that can switch absorption characteristics upon going through a phase change has been reported in a mid-infrared region [18]–[20]. Similarly, various works have focused on the tuning of the reflected power or spectrum accompanied by a phase change of the GST, including an Al nanoantenna based on GST [21]–[23]. However, only a few works have considered the diffraction characteristics in GST-based structures when the structure is pixelated. Such diffraction characteristics are very important, especially when incorporating a GST-based spatial light modulation scheme into diffractive optical applications such as computer-generated holography (CGH). It has been shown that a high diffraction efficiency compared to the portion of non-diffracted light is needed for a clear CGH image reconstructed from the diffractive pattern generated using SLM [24].

Various techniques in nanophotonics have been recently reported, such as micro electro-mechanic systems (MEMS) [25], metasurfaces [26], highly doped transparent semiconductors [27], and graphene photonics [28], and they have also been extensively studied by many researchers for the development of tunable pixel systems and holography. However, those systems still have drawbacks that affect their ability to perfectly replace the conventional SLMs. For example, MEMS suffer from reduced unit pixel size, and it is not easy to apply graphene photonics in the visible light region. Compared to these techniques, GST-based active grating may have its own potential both in highly integrated and visible-light controllable characteristics.

Therefore, in this paper, we investigate and optimize the diffraction characteristics from a few micrometer-sized GST-based line pixels. First, we measured the optical constants of a thin GST film, such as the refractive index and extinction coefficients, using an ellipsometer system for the amorphous and crystalline states of the film. Next, we designed a GST-based line pixel structure by performing a numerical simulation. To do this, we applied the measured optical constants of a GST film. Diffraction from a line pixel is governed by the phase-change of a thin-film GST layer. The results showed that the diffraction efficiency can be significantly increased when a GST layer is encapsulated within two dielectric regions, and is maximized when the GST film is located at the antinodes of the Fabry–Perot (FP) resonance inside the dielectric layers. Such characteristics can be explained by a strong optical phase shift owing to the disturbance of the absorption resonance inside the dielectric region, which strongly enhances the diffraction efficiency caused by a change in GST. The structure can be designed as either broadband or color-selective by tuning the thicknesses of the upper and lower dielectric layers. Furthermore, we also show that we can achieve four different phases of reflected light using a double stack of GST layers insulated through an oxide region. We expect that the use of such multiple phases of diffracted signals may be a promising technique for demonstrating a high-resolution, low-noise CGH image.

II. Measured Optical Constants of the $Ge_2Sb_2Te_5$ Layer

Prior to considering the diffraction characteristics of GST-based line pixels, we briefly show the optical constants of the GST layer that we used in the numerical simulations. As shown in Fig. 1(a), GST has phase-change characteristics between amorphous and crystalline states. When a GST layer is initially sputtered on a flat Si or metal surface, the layer has an amorphous state. Annealing of the GST layer in a furnace at over 150 °C converts the layer into a crystalline state [8]. To return the layer to an amorphous state, heating at about 600 °C followed by rapid cooling are needed to completely melt and cool the GST layer into an amorphous state. The phase-change process is repeatable, and it can be controlled by electrical Joule heating or direct laser illumination [9], [10].

Figures 1(b) and 1(c) show the refractive index and extinction-coefficient profiles of the GST layer used in our calculation. We experimentally measure the parameters using an ellipsometer system (EC-400, J.A. Woollam Co.). The optical constants are fitted using the Cauchy dispersion model from measured reflection and transmission data. We also confirmed that our measurement results show values that are similar to previously reported measurement values for optical constants of GST [29]. We prepared a sample for measuring the

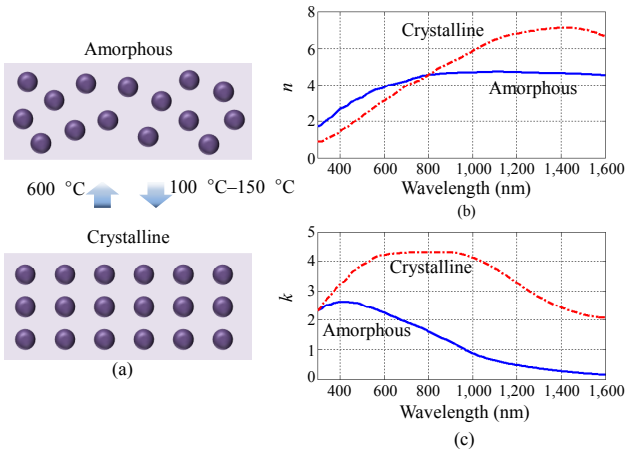

Fig. 1. (a) Plot shows the schematic for the phase-change characteristics of GST and experimentally measured, (b) refractive indexes, and (c) extinction coefficients of the GST layer.

optical constants of an amorphous state by depositing a 20-nm-thick GST layer on a bare Si wafer using a sputter machine. Then, we obtain the parameters for the crystalline state by measuring the sample after annealing in a furnace for 3 h at 190 °C.

With respect to the optical characteristics of a GST layer, first, the change in refractive index within the visible range is very large, but the layer also has high thermal losses. It is very dispersive within the overall range of visible light. Therefore, it will be difficult to directly use a thick GST film as a transparent-type optical device, whereas most researchers have designed GST-based devices as reflection-type devices. Moreover, highly dispersive characteristics have been applied to demonstrate a perfect broadband absorber within the visible and/or near-infrared range [12]. Next, the extinction coefficient of GST is generally higher for the crystalline state, and that of an amorphous state is significantly decreased at a longer wavelength region. Such a low-loss characteristic of GST within the mid-infrared region has been applied to make a tunable absorber [18].

III. Diffraction Characteristic of Line-Pixel GST Structure

1. Line-Pixel Filled by Single GST Layer

Figure 2(a) shows a schematic for simplified two-dimensional reflection-type line pixel. A general display pixel may contain an active cell region, which is spatially localized by the pixel gap (p_{gap}). The active cell region can be designed in several ways, but as shown in Fig. 2(a), we initially show the simplest case in which the cell is only filled by GST. The pixel pitch (Λ_x) is defined as the center-to-center length between nearby pixel gaps. To simplify the diffraction efficiency calculation, we define the 'on' and 'off' states as a periodic change in GST phase states, as shown in the lower and upper parts of Fig. 2(a), respectively.

Figure 2(b) shows the angular diffraction characteristic calculated using the Fourier modal method [30] when the incident light normally illuminates the pixel structure with Λ_x = 2 μm. As shown by the blue bars in Fig. 2(b), the diffraction angles in an "off" state are followed by

$$\theta_{\text{pixel}} = \sin^{-1}\left(\frac{q\lambda_0}{\Lambda_x}\right), \tag{1}$$

where q is an integer value that indicates the diffraction order, and λ_0 is the free space wavelength of incident light. On the other hand, the diffraction angles frequently appear twice for a "pixel on" state because the largest period is doubled. The diffractions for the additional angles, which are shown solely

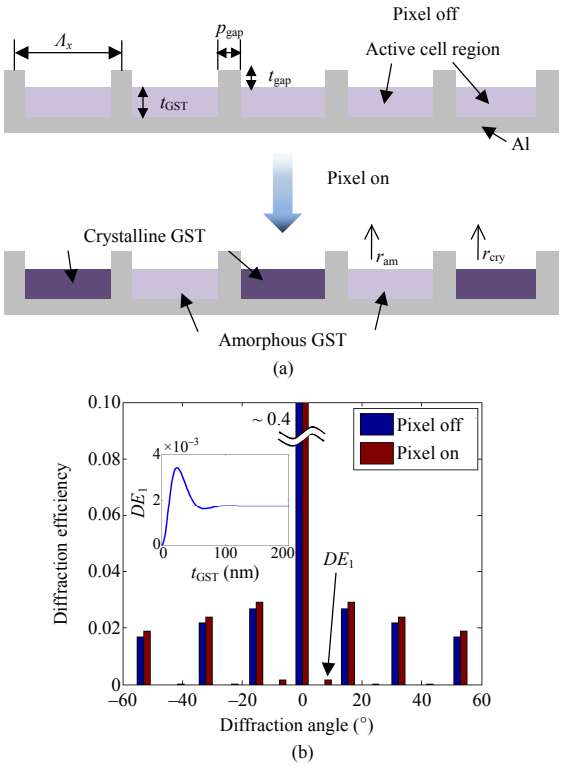

Fig. 2. (a) Schematic of GST-filled line pixel structures for pixel 'on' and off" states. (b) Angular diffraction profile of 'on' and "off" states is shown when the active region is simply filled by 200-nm-thick GST. The inset shows the variation of the DE1 characteristic with the GST film thickness. The detailed simulation parameters are Λ_x = 2 μm, p_{gap} = 400 nm, and t_{gap} = 50 nm.

for a 'pixel on' state, are only affected by the change in the active cell region. For diffractive optical applications such as CGH, the intensity of a hologram image is mainly determined based on the diffraction efficiency (*DE*) caused by the active cell region. Therefore, we need to increase the portion of diffraction caused by a change in GST, which is indicated by the black arrow in Fig. 2(b).

However, when an active cell region is completely filled by a single layer of the GST, the first-order diffraction efficiency in a 'pixel on' state (DE_1) is very small. For a sufficiently thick GST layer, a DE_1 of 0.13% is only achievable, and it cannot exceed 0.35% by simply varying the thickness of the GST region, as shown in the upper-left inset of Fig. 2(b).

When the overall grating height is very small compared to the grating period, we can approximately evaluate the first-order diffraction efficiency of a line-shaped, thin-film-like grating, which has spatially different reflection coefficients r_{am} and r_{cry}, as follows [24]:

$$DE_{\pm 1,\text{ideal}} = \frac{\left|r_{am} - r_{cry}\right|^2}{\pi^2}. \tag{2}$$

From (2), we see that a large $|r_{am} - r_{cry}|$ value is needed for a higher diffraction efficiency, which can be maximized when the conditions $|r_{am}| = |r_{cry}| = 1$ and $|\angle r_{am} - \angle r_{cry}| = \pi$ are achieved. However, the former condition cannot be generally achieved because of the high material loss of GST, as previously mentioned. Nevertheless, the improvement of the diffraction efficiency can be achieved by satisfying the latter condition. For the case of a pixel filled by a single GST layer, a phase difference of $|\angle r_{am} - \angle r_{cry}| = 4.86°$ is achieved, which is too small to expect diffraction caused by the phase difference. Therefore, in the next section, we describe the design of a unit cell geometry that can satisfy the large phase difference by applying dielectric encapsulation layers into the active cell region of a GST-based line pixel.

2. Optimized Unit Cell Geometry with Vertical Cavity Structure

Figure 3(a) shows the unit cell geometry of the proposed pixel structure, where the GST layer is encapsulated by the upper and lower dielectric regions of thickness d_1 and d_2, respectively. Here, we use SiO_2 for the dielectric layer to reduce the unwanted losses and dispersive characteristics that do not originate from the GST layer. Initially, we investigated the effect of the GST thickness. The variation of the diffraction efficiencies of the proposed SiO_2/GST/SiO_2/Al composite pixel layers with the GST thickness and incident wavelength are shown in Fig. 3(b). The figure clearly shows that there is an appropriate range of GST thickness for a high diffraction efficiency of near t_{GST} = 7 nm. In addition, we expect that a GST layer that is too thin cannot sufficiently change the optical reflectance after the material phase change, whereas the absorption of a thick GST layer is too large during a one-time transmission inside the dielectric cavity owing to the large extinction coefficient of the GST layer. Such a large absorption may reduce the resonance characteristic of the cavity, which eventually decreases the phase difference between r_{am} and r_{cry}.

In Figs. 3(c) and 3(d), we also plot the phase and amplitude difference characteristics for different t_{GST} and incident wavelength values to verify that the high diffraction efficiency of the proposed structure mainly originates from the phase difference ($|\angle r_{am} - \angle r_{cry}|$), and not the amplitude difference. It is shown that the high diffraction efficiency conditions directly match the large phase difference in Fig. 3(c).

After determining the appropriate thickness of the GST layer, we aim to optimize the thickness of the upper and lower dielectric layers. Because the embedded GST layer acts as a thin absorption sheet within the dielectric cavity, it is much easier to understand the reflection characteristic by sweeping

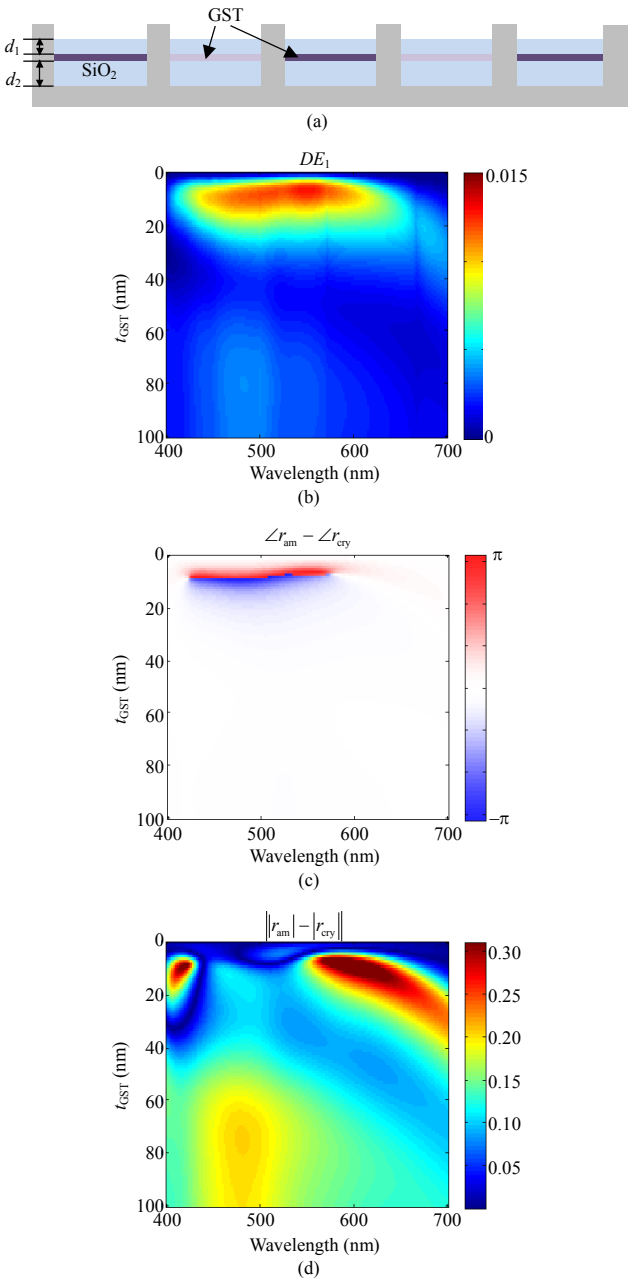

Fig. 3. (a) Schematic of proposed SiO_2/GST/SiO_2/Al composite pixel layers for an 'on' state. (b) First-order diffraction efficiency (DE_1), (c) phase differences, and (d) amplitude difference profiles in accordance with the GST layer thicknesses and incident wavelengths. The thicknesses of the dielectric layers are given as d_1 = 75 nm and d_2 = 75 nm, respectively. The other parameters (Λ_x, p_{gap}, and t_{gap}) are the same as in Fig. 2.

two parameters, namely the overall thickness of the dielectric cavity ($d_{total} = d_1 + d_2$) and the relative position factor of the GST film within the cavity ($P = d_1/d_{total}$).

Figure 4 shows the variation of the diffraction efficiency characteristics of the proposed SiO_2/GST/SiO_2/Al composite

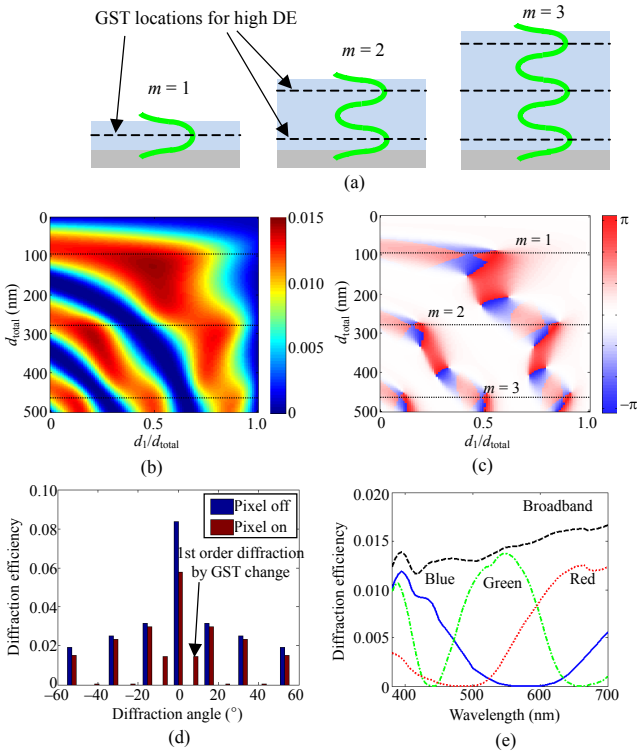

Fig. 4. (a) Schematic showing the appropriate GST film locations within the SiO_2 layer for a high diffraction efficiency. Variation of (b) diffraction efficiency and (c) phase difference characteristics with the total thickness of the SiO_2 layer and relative position factor. (d) Angular diffraction profile of the 'on' and 'off' states for an optimized three-layered structure (d_{total} = 95 nm, P = 0.5). (e) Various SiO_2/GST/SiO_2/Al composite pixel layers for broadband or wavelength-dependent characteristics. Geometric conditions are (d_{total} = 95 nm, P = 0.5) for broadband, (d_{total} = 360 nm, P = 0.5) for blue, (d_{total} = 480 nm, P = 0.1) for green, and (d_{total} = 270 nm, P = 0.45) for red light diffractions.

pixel layers with the two previously mentioned parameters at 532 nm. We see that the thickness of the upper and lower dielectric cavities can significantly affect the diffraction efficiency of the designed structure. When incident light illuminates a pixel, electric fields merge within the dielectric cavity. The positions at which the electric field is strong may vary according to the overall thickness of the dielectric cavity, as depicted in Fig. 4(a). For example, under first-order FP resonance conditions ($d_{total} = \lambda/4n_{SiO_2}$), the maximum electric field can be observed at exactly the middle of the cavity. On the other hand, for the case of second-order FP resonance ($d_{total} = 3\lambda/4n_{SiO_2}$), the appropriate position factor is split into the upper and lower quarters of the cavity. Therefore, we expect that the phase difference of the output signal will be maximized when the thin GST film is located where the electric field is strong. Such an FP resonance-dependent characteristic is clearly shown in Fig. 4(b). By comparing Figs. 4(b) and 4(c), we again confirmed that the high diffraction efficiency conditions are well matched with the large phase difference conditions.

By applying a thin GST film encapsulated by a dielectric cavity, the optimized diffraction efficiency is about 10 times larger than that of a single-layered GST line pixel, as shown in Section III. Figure 4(d) shows the angular diffraction profile of the optimized SiO_2/GST/SiO_2/Al composite pixel layer. Further, it shows that the first-order diffraction efficiency is much stronger compared to that in Fig. 2(b), whereas the zeroth-order reflection is significantly reduced. Moreover, weak second- and third-order diffractions are also observable. Although the absolute *DE* value is not very large (~1.4%) owing to the lossy characteristic of the GST, the first-to-zeroth order diffraction power ratio is significantly improved (~24.8%) compared to the case of Fig. 2(b) (~0.3%). Moreover, the proposed efficiency is sufficient compared to the ideal diffraction grating. It is known that the ideal value of maximum first-order diffraction efficiency for amplitude-modulation-type binary grating (which means 100% reflection for the on-state, whereas it is 0% reflection for the off-state) is about 10%, which is theoretically shown in [24]. We expect that the portion of diffracted light from the GST phase change is clearly observed from the zeroth-order reflection or diffractions caused by the pixel geometry itself.

Considering the practical demonstration of the proposed scheme, the natural oxidation of Al substrate can form an Al_2O_3 layer that is a few nanometers thick. However, the addition of this layer does not significantly change the overall diffraction characteristic because of the broadband characteristic of the diffraction efficiency. For example, we see that the diffraction efficiency is changed from 1.45% to 1.43% when a 5-nm-thick layer of Al_2O_3 is added to the Al surface under the condition of d_{total} = 120 nm, P = 0.5. Moreover, we can recalculate the thin-film resonance condition using the refractive index of Al_2O_3 (about 1.75 at visible light), even for the case of very thick Al_2O_3.

Now, we briefly compare the spectral characteristics of the proposed pixels for different FP resonance conditions, which are shown in Fig. 4(e). Initially, the first-order resonance (m = 1) is not significantly affected by the incident wavelength (black dashed line). Although the geometry is optimized at a 532-nm source, it is clearly shown that *DE* at the blue (440 nm) and red (660 nm) sources is maintained at a similar scale because the other wavelength is also within the range of first-order FP resonance. On the other hand, for higher-order FP resonance conditions (m = 2 or m = 3), the spectral response narrows, as depicted in the other plots of Fig. 4(e). Only a green light source can be diffracted from the pixel structure

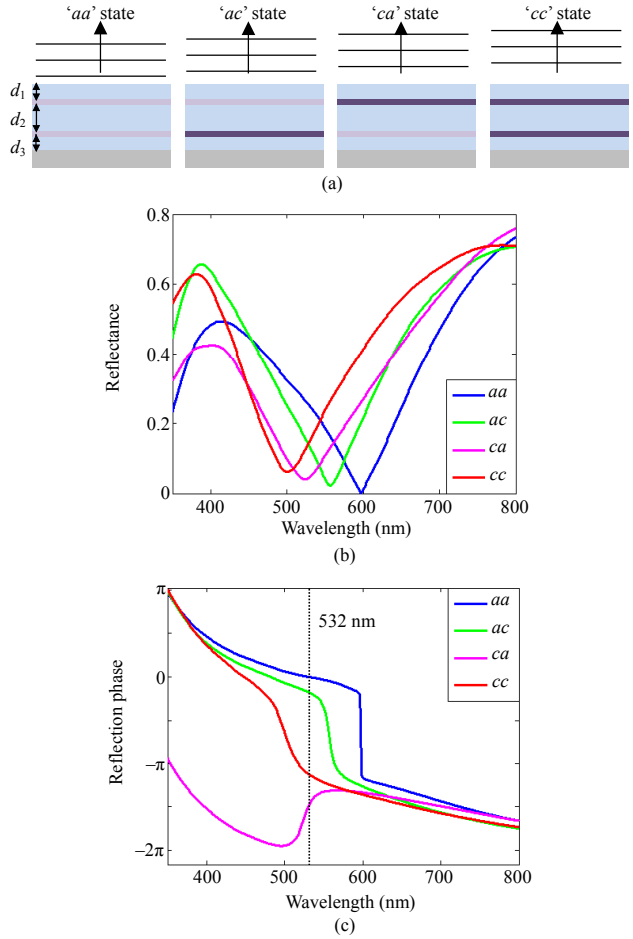

Fig. 5. (a) Schematic of double-stack SiO_2/GST composite layer for multi-level phase generation. (b) Reflection power and (c) phase of reflection coefficient for each state are shown. The reflection phase plots are relative, and are normalized for the '*aa*' state at 532 nm as a zero phase.

when using the third-order FP resonance that is optimized for that wavelength (green dashed-dotted line). Using such a wavelength selectivity at a high-order FP resonance, it is also possible to design diffractive pixel structures that only operate in red and blue light sources, as shown in the red dotted and blue solid lines, respectively. Therefore, we can appropriately design the proposed pixel structure for broadband or specific color applications by tuning the thicknesses of the upper and lower dielectric layers. The detailed geometric conditions for these pixel structures can be found in the caption of Fig. 4.

3. Double-Stack Cavity Structure for Four-Phase Pixel

In the previous section, we investigated whether the material phase change of a thin-film GST layer located at specific locations within the dielectric cavity can dramatically change the phase of the reflection coefficient. We also show that there can be more than two such locations for a higher FP order condition. Therefore, if we insert more than two GST layers into the dielectric cavity and change the material phase of each GST layer separately, it will be possible to control the output reflection phase more than in a binary case. In this section, we show that we can use a double-stack GST film structure to generate four different reflection phases. As shown in Fig. 5(a), two GST films are inserted at the upper and lower parts of the dielectric region, and four states of the GST film are defined as '*aa*,' '*ac*,' '*ca*,' and '*cc*,' according to the state of the GST film. We used d_{total} = 290 nm and positioning factors of $P_{upper} = d_1/d_{total}$ = 0.13 and $P_{lower} = d_3/d_{total}$ = 0.13, which are nearly matched to an m = 2 resonance condition at 532 nm, as depicted in Fig. 4(c). Because the absorption coefficient of GST films is not small, the sum of the upper and lower GST thicknesses should be of the same order of magnitude as the single GST layer introduced in the previous section. We set the upper and lower GST thicknesses to 3.5 nm, which is simply one-half of that in the previous example. Figures 5(b) and 5(c) show the reflection spectra and reflection phase characteristics of each composite film structure shown in Fig. 5(a). From the '*aa*' through the '*cc*' cases, the absorption resonance condition is gradually moved from 600 mm to 500 nm. An abrupt phase shift can be observed under the resonance conditions, which is shown in Fig. 5(c). Interestingly, it is possible to design '*ca*' (magenta line) resonance to an under-coupled resonance, whereas the other cases are over-coupled [31], [32]. Therefore, unlike the other cases, the direction of the phase shift is opposite to that of the "*ca*" case, as shown in Fig. 5(c). Therefore, we can implement four different reflection phases of 0, −0.2π, −1.1π, and −1.5π for each state at 532 nm. We expect that further fine-tuning and iterative optimization of the proposed scheme can bring the output reflection phase closer to the ideal four-phase system (0, −0.5 π, −π, and −1.5π).

IV. Conclusion

In this paper, we proposed the structure for obtaining high diffraction efficiency from a GST-based tunable pixel. By inserting a thin GST film into the antinode positions of the FP resonance of the dielectric layer, the phase of the reflection coefficient can be significantly changed compared to a bare GST film. We confirmed that the high diffraction condition of the proposed structure is mainly dominated by a large phase difference rather than a large amplitude difference. The proposed SiO_2/GST/SiO_2/Al composite pixel layer exhibits a diffraction efficiency that is about 10 times larger, and the first-to-zeroth order diffraction power ratio is 80 times larger compared to the case of the bare GST film. The ~24.8% power ratio of the first-to-zeroth order diffraction may be sufficient for

observing and distinguishing a binary CGH image from the zeroth-order diffraction. By tuning the thicknesses of the dielectric layer, it is possible to design the composite pixel layer working in the broadband region or color selectively within the visible range. We also showed the potential of the proposed scheme in multi-phase applications by inserting more than two GST films into different positions of the dielectric layer. Because the GST-based fabrication processes are already applicable on the sub-micron scale, we expect that the proposed scheme can be applied to develop sub-micron-scale spatial light modulators that can be used for ultra-high resolution CGH applications.

Reference

[1] K.F. MacDonald and N.I. Zheludev, "Active Plasmonics: Current Status," *Laser Photon. Rev*., vol. 4, no. 4, June 2010, pp. 562–567.

[2] N.I. Zheludev and Y.S. Kivshar, "From Metamaterials to Metadevices," *Nat. Mater*., vol. 11, Oct. 2012, pp. 917–924.

[3] M. Seo et al., "Active Terahertz Nanoantennas Based on VO_2 Phase Transition," *Nano Lett*., vol. 10, no. 6, May 2010, pp. 2064–2068.

[4] J.-B. Park et al., "Tunable Subwavelength Hot Spot of Dipole Nanostructure Based on VO_2 Phase Transition," *Opt. Express*, vol. 21, no. 13, July 2013, pp. 15205–15213.

[5] M.A. Kats et al., "Ultra-Thin Perfect Absorber Employing a Tunable Phase Change Material," *Appl. Phys. Lett*., vol. 101, Sept. 2012, pp. 221101-1–221101-5.

[6] K. Appavoo and R.F. Haglund, "Detecting Nanoscale Size Dependence in VO_2 Phase Transition Using a Split-Ring Resonator Metamaterial," *Nano Lett*., vol. 11, no. 3, Feb. 2011, pp. 1025–1031.

[7] Z. Sun, J. Zhou, and R. Ahuja, "Structure of Phase Change Materials for Data Storage," *Phys. Rev. Lett*., vol. 96, no. 5, Feb. 2006.

[8] A.V. Kolobov et al., "Understanding the Phase-Change Mechanism of Rewritable Optical Media," *Nat. Mater*., vol. 3, Sept. 2004, pp. 703–708.

[9] M.H.R. Lankhorst, B.W.S.M.M. Ketelaars, and R.A.M. Wolters, "Low-Cost and Nanoscale Non-volatile Memory Concept for Future Silicon Chips," *Nat. Mater*., vol. 4, Mar. 2005, pp. 347–352.

[10] W.J. Wang et al., "Nonvolatile Phase Change Memory Nanocell Fabrication by Femtosecond Laser Writing Assisted with Near-Field Optical Microscopy," *J. Appl. Phys*., vol. 98, no. 12, Dec. 2005.

[11] C. Ríos et al., "Integrated All-Photonic Non-volatile Multi-level Memory," *Nat. Photon*., vol. 9, Sept. 2015, pp. 725–733.

[12] T. Cao et al., "Broadband Polarization-Independent Perfect Absorber Using a Phase-Change Metamaterial at Visible Frequencies," *Scientific Rep*., vol. 4, Jan. 2014.

[13] P. Hosseini, C.D. Wright, and H. Bhaskaran, "An Optoelectronic Framework Enabled by Low- Dimensional Phase-Change Film," *Nature*, vol. 511, July 2014, pp. 206–211.

[14] N. Konforti, E. Marom, and S.T. Wu, "Phase-Only Modulation with Twisted Nematic Liquid-Crystal Spatial Light Modulators," *Opt. Lett*., vol. 13, no. 3, 1988, pp. 251–253.

[15] S.A. Goorden et al., "Superpixel-Based Spatial Amplitude and Phase Modulation Using a Digital Micromirror Device," *Opt. Express*, vol. 22, no. 15, July 2014, pp. 17999–18009.

[16] H. Bhaskaran et al., "Nanoscale Phase Transformation in $Ge_2Sb_2Te_5$ Using Encapsulated Scanning Probes and Retraction Force Microscopy," *Rev. Sci. Instrum*., vol. 80, Aug. 2009.

[17] H. Satoh, K. Sugawara, and K. Tanaka, "Nanoscale Phase Changes in Crystalline $Ge_2Sb_2Te_5$ Films Using Scanning Probe Microscopes," *J. Appl. Phys*., vol. 99, no. 2, Jan. 2006, pp. 024306-1–024306-7.

[18] T. Cao et al., "Mid-Infrared Tunable Polarization-Independent Perfect Absorber Using a Phase-Change Metamaterial," *J. Opt. Soc. America B*, vol. 30, no. 6, June 2013, pp. 1580–1585.

[19] T. Cao et al., "Rapid Phase Transition of a Phase-Change Metamaterial Perfect Absorber," *Opt. Mater. Express*, vol. 3, no. 8, Aug. 2013, pp. 1101–1110.

[20] A. Tittl et al., "A Switchable Mid-Infrared Plasmonic Perfect Absorber with Multispectral Thermal Imaging Capability," *Adv. Mater*., vol. 27, no. 31, Aug. 2015, pp. 4597–4603.

[21] A.K.U. Michel et al., "Using Low-Loss Phase-Change Materials for Mid-Infrared Antenna Resonance Tuning," *Nano Lett.*, vol. 13, no. 8, June 2013, pp. 3470–3475.

[22] A.K.U. Michel et al., "Reversible Optical Switching of Infrared Antenna Resonances with Ultrathin Phase-Change Layers Using Femtosecond Laser Pulses," *ACS Photon.*, vol. 1, no. 9, Aug. 2014, pp. 833–839.

[23] W. Dong et al., "Wideband Absorbers in the Visible with Ultrathin Plasmonic-Phase Change Material Nanogratings," *J. Phys. Chem. C*, vol. 120, no. 23, June 2016, pp. 12713–12722.

[24] S.A. Benton and V.M. Bove Jr., *Holographic Imaging*, Hoboken, NJ, USA: John Wiley & Sons, 2008.

[25] X. Liu and W.J. Padilla, "Dynamic Manipulation of Infrared Radiation with MEMS Metamaterials," *Adv. Opt. Mater.*, vol. 1, no. 8, June 2013, pp. 559–562.

[26] S.-Y. Lee et al., "Polarization-Multiplexed Plasmonic Phase Generation with Distributed Nanoslits," *Opt. Express*, vol. 23, no. 12, June 2015, pp. 15598–15607.

[27] H.W. Lee et al., "Nanoscale Conducting Oxide PlasMOStor," *Nano Lett.*, vol. 14, Oct. 2014, pp. 6463–6468.

[28] X. Li et al., "Athermally Photoreduced Graphene Oxides for Three-Dimensional Holographic Images," *Nat. Commun.*, vol. 6, Apr. 2015, pp. 1–7.

[29] J.-W. Park et al., "Optical Properties of Pseudo Binary GeTe, $Ge_2Sb_2Te_5$, $GeSb_2Te_4$, $GeSb_4Te_7$, and Sb_2Te_3 from Ellipsometry and Density Functional Theory," *Phys. Rev. B*, vol. 80, 2009,

pp. 115209-1–115209-14.
[30] H. Kim, I.M. Lee, and B. Lee, "Extended Scattering-Matrix Method for Efficient Full Parallel Implementation of Rigorous Coupled-Wave Analysis," *J. Opt. Soc. America A*, vol. 24, no. 8, Aug. 2007, pp. 2313–2327.
[31] J.W. Yoon et al., "Critical Coupling in Dissipative Surface-Plasmon Resonators with Multiple Ports," *Opt. Express*, vol. 18, no. 25, Nov. 2010, pp. 25702–25711.
[32] J.W. Yoon et al., "Surface-Plasmon Mediated Total Absorption of Light into Silicon," *Opt. Express*, vol. 19, no. 21, Oct. 2011, pp. 20673–20680.

Seung-Yeol Lee received his PhD degree in 2014 from the Seoul National University, Rep. of Korea, after which he was a post-doctoral researcher for about two years in the Optical Engineering and Quantum Electronics lab, also at the Seoul National University. Then, he was a researcher at the ETRI, Daejeon, Rep. of Korea for eight months until August 2016. He is currently an assistant professor in the School of Electronics Engineering at the Kyungpook National University, Daegu, Rep. of Korea. His research topics are plasmonics, integrated optics, metasurfaces, and digital holography.

Han Na Kim received her Master's degree in 2016 from the University of Science and Technology, Daejeon, Rep. of Korea, for research in advanced device engineering. She was a researcher at the ETRI, Daejeon, Rep. of Korea, until August 2016. Her research topics are electrochromic device, nanostructures, and digital holography.

Yong Hae Kim received the BS, MS, and PhD degrees in physics from the Korea Advanced Institute of Science and Technology, Daejeon, Rep. of, Korea, in 1991, 1993, and 1997, respectively. From 1997 to 2001, he worked as a research engineer at Hynix Semiconductor, Icheon, Rep. of Korea and was involved in the development of DRAM devices. He has been with the ETRI, Daejeon, Rep. of Korea from 2001, and his current research interests are spatial light modulators, 3D display systems, and metamaterials.

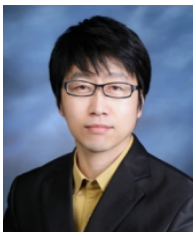

Tae-Youb Kim received his MS degree in physics from Yonsei University, Seoul, Rep. of Korea, in 2000 and his PhD in electronic engineering from Tohoku University, Sendai, Japan, in 2011. He has been with the ETRI, Daejeon, Rep. of Korea as a principal researcher since 2000. His current research interests include electrochromic devices, holographic displays, and sensor devices.

Seong-Mok Cho received his BS, MS, and PhD degrees in materials engineering from the Pohang University of Science and Technology, Rep. of Korea, in 1992, 1994, and 2001, respectively. From February 1994 to January 1996, he worked as a research engineer with the Semiconductor Division of Samsung Electronics, Kiheung, Rep. of Korea. He has been with the ETRI, Daejeon, Rep. of Korea as a principal researcher since 2001. His current research interests include electrochromic devices, holographic displays, and sensor devices.

Han Byeol Kang received the BS degree from the Department of Advanced Materials Engineering for Information and Electronics, Kyung hee University, Yongin, Rep. of Korea, in 2016, where he is currently pursuing the MS degree.

Chi-Sun Hwang received his BS degree in physics from Seoul National University, Rep. of Korea, in 1991 and his PhD in physics from the Korea Advanced Institute of Science and Technology, Daejeon, Rep. of Korea, in 1996. From 1996 to 2000, he worked on DRAM devices with 0.18-μm technology at Hyundai Semiconductor Inc., Incheon, Rep. of Korea. Since 2000, he has been with the ETRI, Daejeon, Rep. of Korea. His research interests include display technology based on active matrix flat panel displays using TFTs, especially oxide TFTs, environment-adaptive displays, digital holography, and novel switching devices.